Iran J Nucl Med. 2023;31(2):119-128 [Serial No. 61]

Homepage: https://irjnm.tums.ac.ir/

ORIGINAL RESEARCH ARTICLE

A Monte Carlo study on quantification of scattering and edge penetration in a breast-dedicated SPECT scanner with lofthole collimation

Maryam Saed[1], Alireza Sadremomtaz[1], Hojjat Mahani[2]

[1]*Department of Physics, Faculty of Science, University of Guilan, Rasht, Iran*

[2]*Radiation Applications Research School, Nuclear Science and Technology Research Institute, Tehran, Iran*

ARTICLE INFO

Article History:
Received: 21 September 2022
Revised: 31 January 2023
Accepted: 06 February 2023
Published Online: 24 April 2023

Keyword:
Penetration
Scattering
SPECT
Collimator
Monte Carlo simulation
Lofthole

*Corresponding Author:
Dr. Alireza Sadremomtaz
Address: Department of Physics, Faculty of Science, University of Guilan, P.O. Box: 41635-1914, Rasht, Iran
Email: sadremomtaz@yahoo.co.uk

ABSTRACT

Introduction: Quantitative accuracy in SPECT is mainly affected by collimator penetration and scattering, particularly for high-energy imaging. Lofthole collimation offers superior performance in terms of penetration and scattering.
Methods: In this research, the GATE Monte Carlo simulator was exploited to calculate edge penetration and scattering in the lofthole collimator using an in-air and in-phantom point source of Tc-99m and I-123. The performance of the lofthole was then compared to that of a pinhole. Both lofthole and pinhole collimators were assumed to have the same geometry including an aperture diameter of 3.04 mm and an opening angle of 75°. Furthermore, the angular distribution of the scattering and penetration were investigated for a multi-lofthole collimator.
Results: The results show that penetration, scattering, and sensitivity are all a function of the photon energy. The penetration and scattering of the pinhole are about 4% higher than that of the lofthole collimator, for Tc-99m SPECT. Compared to the Tc-99m, I-123 SPECT suffers from approximately 1.5- and 1.42-fold higher penetration and scatter fractions, respectively, for lofthole aperture. Moreover, the lofthole collimator presents a higher sensitivity compared with the pinhole (0.030 versus 0.023 for the Tc-99m SPECT). In addition, the findings exhibit a reduction in sensitivity by increasing the photon incidence angle. Both scattering and penetration fractions illustrate a decreasing trend across the angle of incidence.
Conclusion: Compared to pinhole, the lofthole offers superior performance in terms of scattering and penetration for both low- and high-energy SPECT imaging.

Use your device to scan and read the article online

How to cite this article: Saed M, Sadremomtaz A, Mahani H. A Monte Carlo study on quantification of scattering and edge penetration in a breast-dedicated SPECT scanner with lofthole collimation. Iran J Nucl Med. 2023;31(2):119-128.

https://doi.org/10.22034/IRJNM.2023.129010.1533

INTRODUCTION

Single-photon emission computed tomography (SPECT) can probe several functional processes of the object being imaged and therefore has found various applications in cardiac, renal, bone, and breast imaging to detect and diagnose diseases and cancers [1-5]. It is well-known that the collimator plays a key role in the design of such scanners in order to obtain high-quality images [6-10]. Therefore, different generations of collimators have been proposed to balance the existing sensitivity-resolution compromise depending on the imaging task [11-13]. For example, multi-pinhole collimators are widely used in high-resolution imaging where the organ/object of interest is small such as preclinical imaging and breast-dedicated scanning [14-28]. However, SPECT images suffer from collimator scattering and penetration, particularly for high-energy imaging [29, 30]. The problem is approached by introducing new versions of pinhole including keel-edge pinhole [31] and lofthole [9]. Utilizing high-density and high-Z materials such as gold and depleted uranium has been also persuaded [32]. Lofthole has been proposed as a replacement for pinhole as it offers more sensitivity without compromising spatial resolution. Because of the rectangular entrance/exit of the loftholes, they are more compatible with existing rectangular radiation detectors and thereby full detector coverage is affordable.

Cot et al. [33], in 2002, investigated the scattering and septal penetration in fan-beam collimators using Monte Carlo (MC) simulation. Their results showed that for Tc-99m imaging, the geometric component is about 95%, whereas the septal penetration component was 3.7%. Shafaei et al. [30], in 2009, calculated the scattering and septal penetration components in a parallel-hole collimator for an energy range of 250 to 450 keV in a SPECT. They showed that 64% of events in the photopeak window are either scattered or penetrated photons. Dewaraja et al. [34], in 2000, estimated the scattering and edge penetration in parallel-hole collimator for I-131 SPECT. Their simulations showed that 73% of events in the photopeak window had either scattered or penetrated in the collimator, indicating the significance of collimator interactions. In 2019, Konik et al. [29], compared the penetration and scattering in the parallel-hole, single-pinhole, and multi-pinhole collimators using MC simulation. They showed that multi-pinhole collimators provide low penetration and scatter counts compared to parallel-hole collimators. The penetration events for the parallel hole were 14 times higher than that of the multi-pinhole within the 15% photopeak window.

MC simulation is gaining substantial interest in nuclear medicine imaging and dosimetry. MC modeling is the only possible approach for those applications where measurements are not feasible or where analytic models are not available due to the complex nature of the problem [35, 36]. Many general-purpose toolkits like MCNP/MCNPX [37], GEANT4 [38], or dedicated simulators such as GATE [39, 40] have been developed aiming to provide accurate results. GATE has been designed as an upper layer of the GEANT4 and is a dedicated MC software for emission/transmission tomography [7, 41], radiation dosimetry, and radiotherapy with photon, electron, and charged-particle beams [42].

While several publications are centered on the quantification of scattering and edge penetration in pinhole apertures, the literature is scant on the lofthole. As the utilization of lofthole apertures is increasing, there is a need for performance evaluation of such apertures. Therefore, this work aims at characterizing the lofthole collimator in terms of scattering and penetration for two common radionuclides using accurate MC simulation and modeling. To this end, the performance of the lofthole is compared with that of the pinhole as well as analytical derivations.

METHODS

The scanner with lofthole collimation

A breast-dedicated SPECT scanner with lofthole collimation has been previously designed and optimized by the authors [22]. The scanner has a cylindrical field-of-view (FOV) allowing breast SPECT imaging in a step-and-shoot manner with two steps. Key technical details of the collimator are listed in Table 1. All holes are distributed over a single full ring. Moreover, the apertures are focused toward the center of the FOV with any tilting. A monolithic NaI(Tl) crystal, with an intrinsic resolution of 3.2 mm, was considered as a scintillation detector which was a square with dimensions of 80×80 mm2 and 10 mm in thickness. For a fair comparison (as discussed later), the loftholes were also replaced with pinhole ones with the same specifications. Figure 1 illustrates the two setups corresponding to lofthole and pinhole collimations.

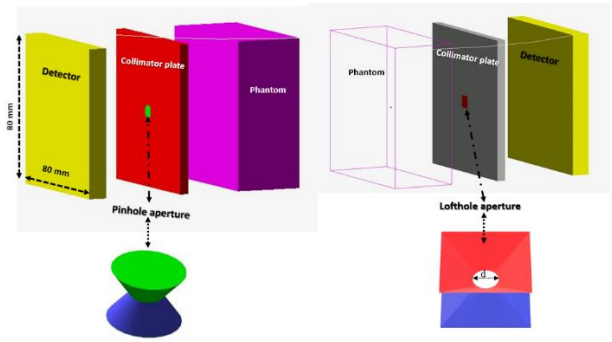

Fig 1. Schematics of single-lofthole (back-to-back pyramid) (right) and single-pinhole (back-to-back cone) (left) apertures in GATE simulation.

Table 1. Key technical details of breast-dedicated SPECT scanner

Parameters	Value
Collimator material and thickness	Tungsten, 5 mm
Collimator-to-source distance	47 mm
Detector-to-source distance	95 mm
Detector material and thickness	NaI(Tl), 10 mm
Lofthole opening angle	75°
Lofthole diameter	3.04 mm

Monte Carlo simulation

An MC study was carried out using the GATE version 8.2 simulator [40]. In this work, all the relevant radiation physics including photoelectric absorption, Compton and Rayleigh scattering for gamma-rays, as well as ionization, Bremsstrahlung, and multiple scattering for electrons were modeled. Cut-off values of 0.1 cm and 1.0 cm for photons and electrons, respectively, in the head of the scanner, were considered. The detector's energy resolution was assumed to be energy-dependent, Gaussian-distributed, where the full-width at half maximum (FWHM) was 10% of a photon's energy [43, 44]. Energy windows according to Table 2 were applied to the simulation results. Also, the intrinsic spatial resolution of the detector was taken into consideration [39]. ROOT version 6.15 was exploited for MC simulation analysis. The ROOT is an object-oriented data analysis framework with all the functionality needed to handle and analyze large amounts of data in a very efficient way [45]. The statistical uncertainties of the MC simulations were below 1.0%.

Table 2. Settings of the 20% energy windows for different isotopes

Tracer	Photopeak (keV)	Photopeak window (keV)
Tc-99m	140	126-154
I-123	159	143-175

Quantification of collimator scattering and penetration

Edge penetration and scattering were calculated using a set of GATE simulations. The simulations were performed with an in-air point source located at the center of the FOV using two commonly used radionuclides: Tc-99m and I-123. As collimator scattering and penetration cannot be directly calculated using GATE, a C++ script was developed to extract the desirable information from the ROOT output. The total detected counts include direct, penetration, and scattered photons. The primary count is a mixture of direct and penetrated photons. Direct photons are defined as the unscattered events that reach the detector and are counted within the energy window. Edge penetration is defined as the percentage of photons passing through the lofthole/pinhole edges without any interaction with the edges and then being

detected within the energy window. These photons may or may not have scattered in places other than the collimator before or after collimator penetration. The scattered photons are those subjected to a single or multiple Compton or Rayleigh scattering with matter prior to detection within the defined energy window. That is, the scattered photons not reaching the crystal or being outside the energy window are not counted as scattered photons.
For calculations, only a single-hole was modeled. To separate the direct and penetration from the primary count, two series of MC simulations were performed. In the first set, both photons passing directly through the aperture (direct) and those passing through the collimator material (penetration) were recorded. In the second simulation, only those photons passing through the collimator materials (penetration) were recorded by filling the holes with a virtual ultra-high-Z and ultra-high-density material. By subtracting the penetration contribution from all events, it is feasible to calculate the direct component. All simulated data were acquired considering a 20% energy window (see Table 2). A data acquisition period of 5 min with 1 MBq Tc-99m/I-123 was considered for each collimator setup.

Angular distribution of scattering and penetration

To evaluate the angular dependency of scattering and edge penetration, the point source was placed at 6 different positions across line S to fully cover the axial FOV of the scanner. The positions of the point source were 0, 2, 5, 8, 16, and 24 mm where 0 denotes the position of the point source at the center of FOV. The corresponding angles for each position were 0, 2.43, 6.07, 9.56, 18.79, and 27.05 degrees, respectively. An 8-hole collimator was considered for the calculation of the angular distribution of the scattering and penetration. Figure 2 displays the positions of the point source over line S. The simulations were performed with an in-air 2 MBq Tc-99m point source. The simulations were repeated for such a source in the breast-mimicking phantom, as well. The breast phantom was a cylinder with 72 mm in diameter and 72 mm in height (equal to the FOV of the scanner). The data acquisition was considered for 300 s. By replacing the loftholes with pinholes of the same geometries, the GATE simulations were repeated for a multi-pinhole-collimated scanner. Figure 3 is a view of a multi-pinhole collimator modeled in the GATE.

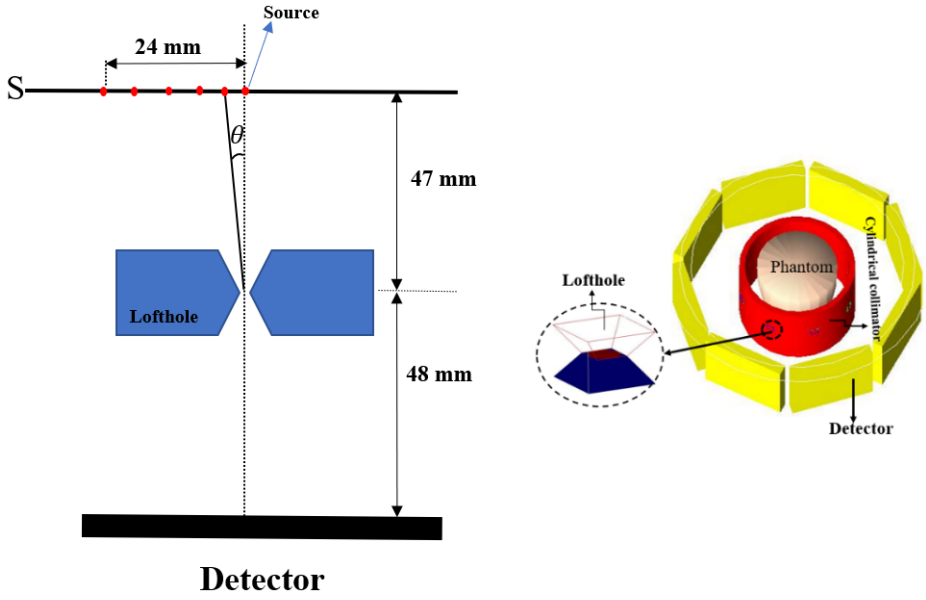

Fig 2. 3D view, not to scale, of the SPECT scanner with eight-lofthole (right); Position of the point-source over the line S with respect to the collimator/detector assembly (left)

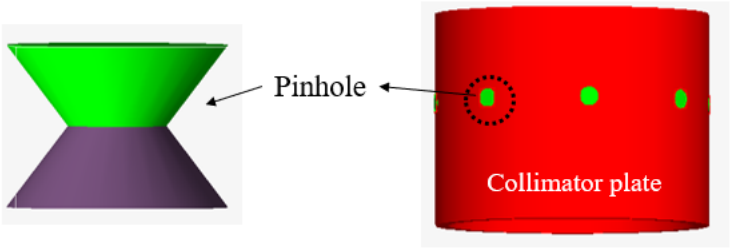

Fig 3. The view of the multi-pinhole collimator designed in the GATE simulator

Comparison with analytical derivations

For the pinhole, Metzler et al. [46], analytically derived the scattering and penetration of the collimator. Because the lofthole is a new version of pinhole, the finding of this study was compared with those of Metzler's formula to investigate whether a pinhole-based derivation works well for lofthole collimators. For a fair comparison, we used an in-air point source with a problem geometry identical to Metzler's assumption. Sensitivity was considered as the fraction of photons emitted from a point source reaching the detector surface. The total sensitivity consists of two components: (1) geometric and (2) penetration sensitivities. Geometric sensitivity is a fraction of emitted photons that pass through the aperture and do not suffer attenuation; penetration sensitivity is defined as the ratio of photons passing through the attenuating medium of the collimator to emitted photons. Metzler et al. [46] formulated these two components as follows:

$$S_{geo}(\varphi) = \frac{d^2}{16h^2} \times \sin^3 \varphi \qquad (1)$$

$$S_{pen}(\varphi) = \frac{\sin^3 \varphi}{4h^2 \acute{a}} \frac{(2+\acute{a}d)}{(1+\gamma)^{\frac{1}{2}}} \qquad (2)$$

where d is the physical diameter of the aperture, h is the normal distance of source to lofthole (in our scanner, 47 mm), and φ is $\frac{\pi}{2} - \theta$. Moreover, $\acute{a}$ and γ are:

$$\acute{a} = \frac{2\mu \tan\frac{\alpha}{2}}{(\tan^2\frac{\alpha}{2} - \cot^2 \varphi) \sin \varphi} \qquad (3)$$

$$\gamma = \frac{\cot^2 \varphi}{tan^2(\frac{\alpha}{2})} \qquad (4)$$

here μ is the linear attenuation coefficient of tungsten at 140 keV (3.39 mm-1), and α is the opening angle. The total analytical sensitivity is obtained by summing Eqs. 1 and 2.

RESULTS

Comparison of pinhole and lofthole collimators

Scattering and edge penetration

Quantitative results of scattering and edge penetration in lofthole and pinhole apertures, for two radiotracers, I-123 and Tc-99m, are listed in Table 3. Percentage edge penetration and scattering are estimated in terms of fractions with respect to the total count. Also, the ratio of total detected photons to emitted photons is reported as sensitivity.

Table 3. Comparison scattering, penetration (as a percent of the total detected photon), and sensitivity in lofthole and pinhole collimators for two radiotracers

	Tc-99m		I-123	
	Lofthole	**Pinhole**	**Lofthole**	**Pinhole**
Scattering (%)	0.1211	0.1272	0.21	0.24
Penetration (%)	14.00	14.59	21.07	21.12
Sensitivity (%)	0.030	0.023	0.028	0.022

Angular distribution of scattering and penetration

In Figure 4, the total GATE MC simulated in-air sensitivity for the Tc-99m point source is compared to the theoretical formula (Metzler's derivation) as a function of the angle of incidence photon.

Figure 5 plots the sensitivity components obtained from in-air Tc-99m point source for various angles. In the graph, geometric sensitivity has been calculated as the ratio of the direct photons to emitted ones extracted from the GATE simulation. Likewise, penetration sensitivity has been defined as the ratio of penetrated photons to emitted ones.

Figure 6 shows the percentage scatter fraction as a function of the angle of incidence photon (θ) using GATE simulations for multi-lofthole and multi-pinhole collimators. The collimator scatter was obtained from the ROOT output for the in-air Tc-99m point source.

Figure 7 manifests the collimator penetration fraction and total sensitivity in percent as a function of the angle of incidence photon (θ) for in-air as well as in-phantom 2 MBq Tc-99m point source.

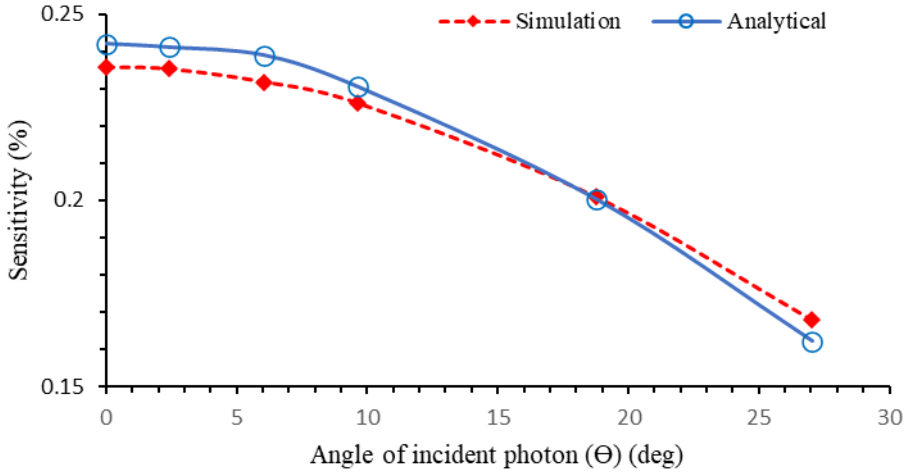

Fig 4. Comparison of theoretical and simulated total sensitivity as a function of the angle of the incidence photon (Θ)

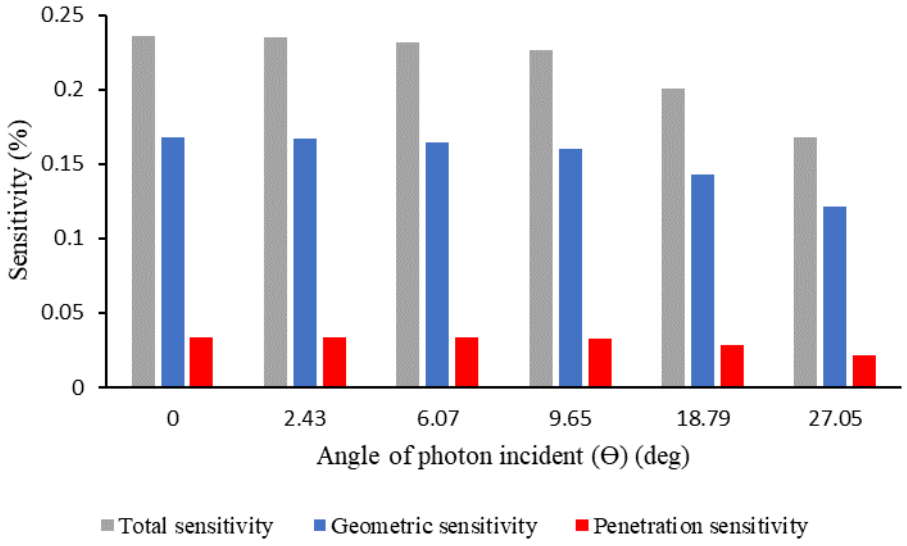

Fig 5. System sensitivity, geometric sensitivity, penetration sensitivity as a function of angle of incidence photon (Θ) in multi-lofthole collimator for Tc-99m tracer

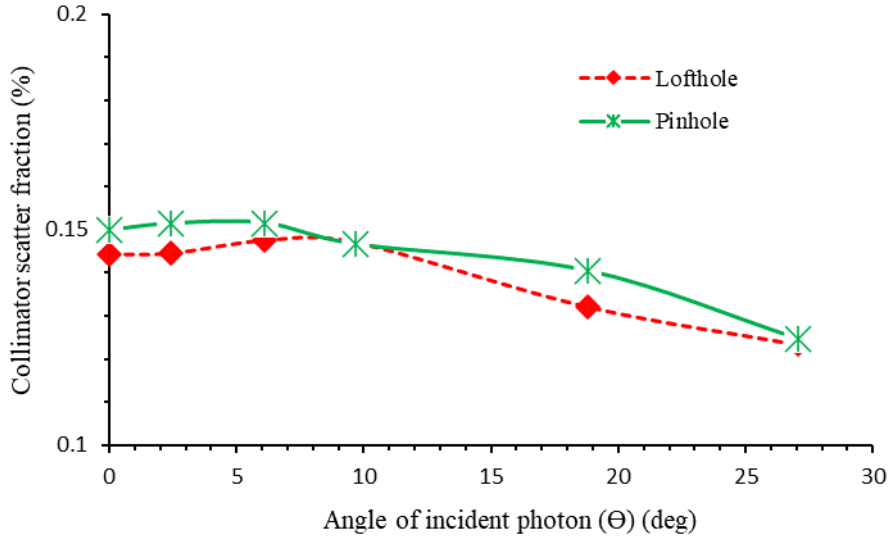

Fig 6. In-air scatter fraction for lofthole and pinhole as a function of angle of incidence photon (θ) for Tc-99m SPECT

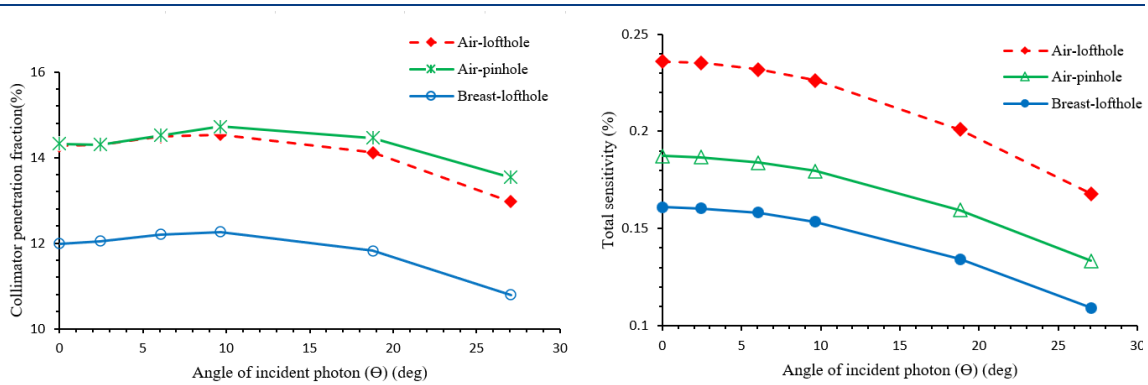

Fig 7. In-air and in-phantom collimator penetration fraction (left) and total sensitivity (right) as a function of angle of incidence photon (θ) for the lofthole and pinhole collimations

DISCUSSION

According to Table 3, penetration and scattering for I-123 are considerably higher than those of Tc-99m for both collimators. Penetration is 21.07% of the total counts for I-123 SPECT with lofthole collimation. The corresponding value for pinhole SPECT is 21.12%. When Tc-99m is used, penetration is 14% and 14.59% of the total detected photons in lofthole and pinhole collimators, respectively. Referring to Table 3, the sensitivity is higher for both radiotracers with lofthole collimation compared to the pinhole aperture.

As listed in Table 3, the scattering and penetration of the lofthole are lower than those of the pinhole. For example, in Tc-99m pinhole SPECT, penetration and scattering are about 4% higher than in the lofthole collimator. This is mainly due to the shape of the lofthole exit. Compared to the Tc-99m, I-123 SPECT suffers from approximately 1.5- and 1.42-fold higher penetration and scatter fraction, respectively, for the lofthole aperture. This is because of the higher energy of I-123 compared to Tc-99m. Furthermore, the system sensitivity is higher using the lofthole collimator [29, 46-48]. For instance, the sensitivity of the pinhole is about 27% lower than that of the lofthole in I-123 SPECT. As previously mentioned, due to the rectangular projections of the lofthole collimator, 100% of the detector surface can be covered resulting in higher sensitivity. The sensitivity decreases with increasing the photon energy from 140 keV to 159 keV (0.03% versus 0.028% for lofthole). The reason can be explained that by increasing the energy, the contribution of scattered and penetrated

photons also increases while the contribution of direct photons decreases mainly due to the lower detection efficiency of NaI (Tl) crystal in higher energies. For example, the ratio of penetrated photons to the direct ones is 34% for I-123 while this value was 19% for Tc-99m.

According to Figure 4, both simulated and analytical sensitivity depends on the angle of incidence photon. Thus, the sensitivity for the 0° incidence angle is about 29% higher than that of the 27° incidence angle in the multi-lofthole. In Figure 5, all three sensitivity components decrease with increasing the angle of incidence. For instance, the total sensitivity at θ equal to 0° is 0.23%, whereas the corresponding value at 27° is 0.16%. At angles 0° and 27°, the magnitudes of geometric sensitivity are 0.16% and 0.12% and corresponding values for penetration sensitivity are 0.033% and 0.021%, respectively.

Referring to Figure 4, the findings of this study confirm that Metzler's model works well for lofthole collimators with a relative error of less than 5% at all angles. The main origin of such difference is that in Metzler's formula, a perfect detector (with a detection efficiency of 100%) has been assumed, while a realistic detector is considered in this work. By increasing the photon incidence angle, the total sensitivity decreases, which is mostly due to the reduction of scattering and penetration components. As can be seen in Figure 5, the total sensitivity at a perpendicular angle (Θ equal 0°) is higher than the total sensitivity at 27°, due to the greater contribution of penetrated photons.

Figures 6 and 7 show the angular dependence of the scattering and the penetration for in-air point source simulation, respectively. It can be seen that increasing the angle (i.e., θ) leads to a reduction in the collimator scattering and penetration, which results in a decreased total sensitivity. This situation is also observed for the pinhole, but with a difference that the amount of scattering and penetration is higher, and the sensitivity is lower at all angles. As mentioned, this is due to the shape of the lofthole exit. According to Figures 6 and 7, the scattering and penetration fractions increased between the angles of 2 to 10 degrees. In this angular interval, the probability of penetration and scattering is slightly increased as the source is not face-to-face with the hole and therefore the source sees mostly the edges than the holes. For this reason, the contribution of penetrated (and/or scattered) photons is more pronounced than that of direct photons. Further increasing the angle (> 10°), the average path length of photons through the lofthole/pinhole material (both the edges and body) increases, thus reducing the probability of detection of a penetrated/scattered photon.

Compared to the in-air case, detected penetration is approximately 16% lower than for in-phantom simulation at all angles. For example, penetrated photons at an angle of 0° are about 14% for in-air source, while the corresponding value is 12% for in-phantom source. As shown in Figure 7, breast phantom results in lower sensitivity, the reason is the attenuation of the originally emitted photons. The results also show that simulation with an in-phantom source leads to a primary count of about 72% while this value is 85.36% for an in-air source. The reason for the reduction is a 15% scattered photon in the breast phantom.

CONCLUSION

In this study, as a first report on the topic, lofthole collimator scattering and penetration have been characterized using MC simulation. Our results confirm that the lofthole collimator provides superior performance not only in terms of system sensitivity but also in terms of scattering and penetration compared to the pinhole. Higher energy SPECT imaging automatically leads to inferior performance for both collimators but to a lower extent for the lofthole. In addition, the existing pinhole-based derivation for quantification of collimator scattering and perpetration is still valid for the lofthole collimator, as well. Future work is investigating image-based metrics for pinhole and lofthole collimators for both low- and high-energy SPECT.

REFERENCES

1. Savelli G, Maffioli L, Maccauro M, De Deckere E, Bombardieri E. Bone scintigraphy and the added value of SPECT (single photon emission tomography) in detecting skeletal lesions. Q J Nucl Med. 2001 Mar;45(1):27-37.
2. Brem RF, Rapelyea JA, Zisman G, Mohtashemi K, Raub J, Teal CB, Majewski S, Welch BL. Occult breast cancer: scintimammography with high-resolution breast-specific gamma camera in women at high risk for breast cancer. Radiology. 2005 Oct;237(1):274-80.
3. Slomka PJ, Patton JA, Berman DS, Germano G. Advances in technical aspects of myocardial perfusion SPECT imaging. J Nucl Cardiol. 2009 Apr;16:255-76.
4. Piruzan E, Vosoughi N, Mahdavi SR, Khalafi L, Mahani H. Target motion management in breast cancer radiation therapy. Radiol Oncol. 2021 Dec 1;55(4):393-408.
5. Tarighati E, Keivan H, Mahani H. A review of prognostic and predictive biomarkers in breast cancer. Clin Exp Med. 2023 Feb;23(1):1-16.
6. Van Audenhaege K, Van Holen R, Vandenberghe S, Vanhove C, Metzler SD, Moore SC. Review of SPECT collimator selection, optimization, and fabrication for

clinical and preclinical imaging. Med Phys. 2015 Aug;42(8):4796-813.
7. Mahani H, Raisali G, Kamali-Asl A, Ay MR. Spinning slithole collimation for high-sensitivity small animal SPECT: Design and assessment using GATE simulation. Phys Med. 2017 Aug;40:42-50.
8. van der Have F, Ivashchenko O, Goorden MC, Ramakers RM, Beekman FJ. High-resolution clustered pinhole (131)Iodine SPECT imaging in mice. Nucl Med Biol. 2016 Aug;43(8):506-11.
9. Deprez K, Pato LR, Vandenberghe S, Van Holen R. Characterization of a SPECT pinhole collimator for optimal detector usage (the lofthole). Phys Med Biol. 2013 Feb 21;58(4):859-85.
10. Mahani H, Ay MR, Sarkar S, Farahani MH, inventors; Parto Negar Persia Co, assignee. Single photon emission computed tomography imaging with a spinning parallel-slat collimator. United States patent US 10,795,033. 2020 Oct 6.
11. Mahani H, Raisali G, Kamali-Asl A, Ay MR. Collimator-detector response compensation in molecular SPECT reconstruction using STIR framework. Iran J Nucl Med. 2017;25(Supplement 1):26-34.
12. Mahani H, Kamali-Asl A, Ay MR. How gamma camera's head-tilts affect image quality of a nuclear scintigram?. Front biomed technol. 2014 Dec 30;1(4):265-70.
13. Asma E, Manjeshwar R. Evaluation of the impact of resolution-sensitivity tradeoffs on detection performance for SPECT imaging. IEEE Nucl Sci Symp Conf Rec. 2008 Oct 19; 3730-3733
14. Beekman FJ, Vastenhouw B. Design and simulation of a high-resolution stationary SPECT system for small animals. Phys Med Biol. 2004;49(19):4579.
15. Wang H, Scarfone C, Greer KL, Coleman RE, Jaszczak RJ. Prone breast tumor imaging using vertical axis-of-rotation (VAOR) SPECT systems: an initial study. IEEE Trans Nucl Sci. 1997;44(3):1271-6.
16. Weinmann AL, Hruska CB, O'Connor MK. Design of optimal collimation for dedicated molecular breast imaging systems. Med Phys. 2009 Mar;36(3):845-56.
17. Williams MB, Judy PG, Gunn S, Majewski S. Dual-modality breast tomosynthesis. Radiology. 2010 Apr;255(1):191-8.
18. Wang B, van Roosmalen J, Piët L, van Schie MA, Beekman FJ, Goorden MC. Voxelized ray-tracing simulation dedicated to multi-pinhole molecular breast tomosynthesis. Biomed Phys. Eng Express. 2017;3(4):045021.
19. van Roosmalen J, Goorden MC, Beekman FJ. Molecular breast tomosynthesis with scanning focus multi-pinhole cameras. Phys Med Biol. 2016 Aug 7;61(15):5508-28.
20. van Roosmalen J, Beekman FJ, Goorden MC. System geometry optimization for molecular breast tomosynthesis with focusing multi-pinhole collimators. Phys Med Biol. 2017 Dec 19;63(1):015018.
21. Tornai MP, Bowsher JE, Archer CN, Peter J, Jaszczak RJ, MacDonald LR, Patt BE, Iwanczyk JS. A 3D gantry single photon emission tomograph with hemispherical coverage for dedicated breast imaging. Nucl Instrum Methods Phys Res Sect A Accel Spectrom Detect Assoc Equip. 2003;497(1):157-67.
22. Saed M, Sadremomtaz A, Mahani H. Design and optimization of a breast-dedicated SPECT scanner with multi-lofthole collimation. J Instrum. 2022 Jan 4;17(01):P01006.
23. van Holen R, Vandeghinste B, Deprez K, Vandenberghe S. Design and performance of a compact and stationary microSPECT system. Med Phys. 2013 Nov;40(11):112501.
24. van der Have F, Vastenhouw B, Ramakers RM, Branderhorst W, Krah JO, Ji C, Staelens SG, Beekman FJ. U-SPECT-II: An ultra-high-resolution device for molecular small-animal imaging. J Nucl Med. 2009 Apr;50(4):599-605.
25. Tornai MP, Bowsher JE, Jaszczak RJ, Pieper BC, Greer KL, Hardenbergh PH, Coleman RE. Mammotomography with pinhole incomplete circular orbit SPECT. J Nucl Med. 2003 Apr;44(4):583-93.
26. Song TY, Choi Y, Chung YH, Jung JH, Choe YS, Lee KH, Kim SE, Kim BT. Optimization of pinhole collimator for small animal SPECT using Monte Carlo simulation. IEEE Trans Nucl Sci. 2003 Jun;50(3):327-32.
27. Shokouhi S, Metzler SD, Wilson DW, Peterson TE. Multi-pinhole collimator design for small-object imaging with SiliSPECT: a high-resolution SPECT. Phys Med Biol. 2009 Jan 21;54(2):207-25.
28. Paix D. Pinhole imaging of gamma rays. Phys Med Biol. 1967 Oct;12(4):489-500.
29. Könik A, Auer B, De Beenhouwer J, Kalluri K, Zeraatkar N, Furenlid LR, King MA. Primary, scatter, and penetration characterizations of parallel-hole and pinhole collimators for I-123 SPECT. Phys Med Biol. 2019 Dec 13;64(24):245001.
30. Shafaei M, Ay MR, Sardari D, Dehestani N, Zaidi H. Monte Carlo assessment of geometric, scatter and septal penetration components in DST-XLi HEGP collimator. 4th European Conference of the International Federation for Medical and Biological Engineering: ECIFMBE 2008 23–27. November 2008 Antwerp, Belgium 2009: 2479-2482. Springer Berlin Heidelberg.
31. van Der Have F, Beekman FJ. Penetration, scatter and sensitivity in channel micro-pinholes for SPECT: a Monte Carlo investigation. IEEE Trans Nucl Sci. 2006;53(5):2635-45.
32. Nguyen MP, Goorden MC, Beekman FJ. EXIRAD-HE: multi-pinhole high-resolution ex vivo imaging of high-energy isotopes. Phys Med Biol. 2020 Nov 18;65(22):225029.
33. Cot A, Sempau J, Pareto D, Bullich S, Pavia J, Calvino F. Evaluation of the geometric, scatter, and septal penetration components in fan-beam collimators using Monte Carlo simulation. IEEE Trans Nucl Sci. 2002;49(1):12-6.
34. Dewaraja YK, Ljungberg M, Koral KF. Characterization of scatter and penetration using Monte Carlo simulation in 131I imaging. J Nucl Med. 2000 Jan;41(1):123-30
35. Zaidi H. Relevance of accurate Monte Carlo modeling in nuclear medical imaging. Med Phys. 1999 Apr;26(4):574-608.
36. Staelens S, Buvat I. Chapter 5 - Monte Carlo Simulations in nuclear medicine imaging. Verdonck P, editor. Advances in biomedical engineering. Amsterdam: Elsevier; 2009. p. 177-209.
37. Briesmeister JF. MCNPTM-A general Monte Carlo N-particle transport code. Version 4C, LA-13709-M, Los Alamos National Laboratory. 2000; 2.
38. GEANT4. Available from: https://geant4.web.cern.ch/.
39. Jan S, Santin G, Strul D, Staelens S, Assié K, Autret D, Avner S, Barbier R, Bardies M, Bloomfield PM, Brasse D. GATE: a simulation toolkit for PET and SPECT. Physics in medicine and biology. 2004 Sep 10;49(19):4543.
40. OpenGATE Collaboration. Updated on July 01, 2021. Available from: http://www.opengatecollaboration.org/.
41. Mahani H, Raisali G, Kamali-Asl A, Ay MR. How crystal configuration affects the position detection accuracy in pixelated molecular SPECT imaging systems?. Nucl Sci Tech. 2017 Apr;28:1-7.
42. Piruzan E, Vosoughi N, Mahani H. Development and validation of an optimal GATE model for double scattering proton beam delivery. J Instrum. 2021 Feb 18;16(02):P02022.
43. Cherry SR, Sorenson JA, Phelps ME. Physics in Nuclear Medicine. 4th Ed. Philadelphia: Elsevier Inc.; 2012.

44. Knoll GF. Radiation detection and measurement. John Wiley & Sons; 2010.
45. Framework RDA. ROOT Data Analysis Framework. Available from: https://root.cern/.
46. Metzler SD, Bowsher JE, Smith MF, Jaszczak RJ. Analytic determination of pinhole collimator sensitivity with penetration. IEEE Trans Med Imaging. 2001 Aug;20(8):730-41
47. Deloar HM, Watabe H, Aoi T, Iida H. Evaluation of penetration and scattering components in conventional pinhole SPECT: phantom studies using Monte Carlo simulation. Phys Med Biol. 2003 Apr 21;48(8):995-1008.
48. Jung YJ, Kim K, Kim J, Woo SK, Park J, Lee YS, Lee W, Yu JW, Lee K, Kim J. Modeling high energy (I-131) pinhole collimator for small animal gamma ray imaging device by Monte Carlo simulation (GATE 6.0). 2011 IEEE Nucl Sci Conf R. 2011 Oct 23; 2756-2759.